communications biology

A Nature Portfolio journal

Article

https://doi.org/10.1038/s42003-025-07798-2

# Invariant NK T cells counteract HCC metastasis by mediating the migration of splenic CD4$^+$ T cells into the white pulp and infiltration of B cells



Jinke Geng[1,5], Mengxiao Xie[2,5], Meina Yan[1], Xiaoyan Xie[1], Fuxin Wang[3], Rui Zhu[3] ✉ & Mutian Han[1,4] ✉

Despite significant advances in the diagnosis and treatment of hepatocellular carcinoma (HCC), metastasis and recurrence remain two major obstacles to improving the clinical outcomes for HCC patients. Here, we demonstrate that splenic invariant natural killer T (iNKT) cells can significantly inhibit Hepa1-6-mediated intrahepatic HCC metastasis. Interestingly, in the HCC metastasis model, iNKT deficiency can result in a significant decrease in percentage and absolute number of CD4$^+$ T cell and interleukin-4 level, thus suggesting the involvement of the cross-talk between iNKTs and CD4$^+$ T cells in limiting HCC metastasis to the spleen. Transcriptional signatures of CD4$^+$ T cells following iNKT deficiency displaying impairment of their cell migration function. During HCC metastasis, splenic iNKT rapidly secrete interferon-γ to promote the migration of CD4$^+$ T cells from the marginal zone into the white pulp, thereby triggering subsequent migration of splenic B cells to the liver and exerting anti-tumor immune effects on Hepa1-6 cells. In conclusion, interactions between interferon-γ and its receptor on iNKT and CD4$^+$ T cells can effectively coordinate immune activity between the marginal zone and the white pulp, thereby ultimately inhibiting intrahepatic HCC metastasis. These findings reveal the mechanism underlying the resistance of splenic iNKT to tumor metastasis.

Hepatocellular carcinoma (HCC) is the fourth leading cause of cancer-related mortality worldwide and the leading cause of death from liver cirrhosis[1]. With a 5-year survival rate of 18%, HCC is the second deadliest tumor after pancreatic cancer[2]. Although, significant advances have been made both in the diagnosis and treatment of cancer over the past few centuries, but metastasis and recurrence remain the main obstacle to improving clinical outcomes in cancer patients[3]. Despite the availability of various treatment options for the management of HCC patients, such as surgical resection, percutaneous ablation, radiotherapy, and transarterial and systemic therapies, these patients are still at a high risk of tumor metastasis, especially local intrahepatic invasion[4]. Surgical resection, is the recommended treatment option, with a 5-year overall survival rate of ~70%, but a significant drawback of this approach is the high incidence of local invasion by liver tumors[5], occurring in up to 80% of patients[5,6]. The local invasion of cancer is a complex, multi-step process involving infiltration of cancer cells into the primary lesion, entry into the blood stream, survival in the circulation, extravasation and attachment and colonization of the metastatic site[7]. The means by which splenic iNKTs exert immune surveillance of this process remains largely unknown.

The mouse spleen is divided into red pulp (RP) and white pulp (WP) according to function and structure, with the marginal zone (MZ) located between these two areas[8]. In contrast to lymph nodes, the spleen lacks afferent lymphatic vessels and all cells as well as antigens can enter the spleen via the blood. Therefore, RP dominates the spleen tissue, constituting a significant portion, whereas the WP accounts for less than a quarter, but serves as key immunologic region of the spleen[9]. The structure of the spleen

[1]Center for Medical Laboratory Science, Affiliated Suzhou Hospital of Nanjing Medical University, Suzhou Municipal Hospital, Gusu School, Nanjing Medical University, Suzhou, Jiangsu, China. [2]Department of Laboratory Medicine, Jiangsu Province Hospital, Nanjing, Jiangsu, China. [3]Center for Human Reproduction and Genetics, Affiliated Suzhou Hospital of Nanjing Medical University, Suzhou Municipal Hospital, Gusu School, Nanjing Medical University, Suzhou, Jiangsu, China. [4]Center for Research and Experimental, Suzhou Vocational Health College, Suzhou, Jiangsu, China. [5]These authors contributed equally: Jinke Geng, Mengxiao Xie. ✉e-mail: zhurui2528@njmu.edu.cn; Jiopkuy@aliyun.com

allows it to efficiently remove blood-borne microorganisms, older erythrocytes and cellular debris from the circulation, earning it the distinction of being the body's largest blood filter[10]. Moreover, except for red blood cells, all types of blood cells, regardless of the volume can pass through the blood vessels in the spleen for ~10 min[11–13]. This facilitates full contact and interaction between tumor cells and immune cells in the red pulp and marginal zone. Interestingly, numerous studies have reported the beneficial role of the spleen in significantly improving the tumor prognosis. For instance, preservation of the spleen during extended lymphadenectomy for gastric cancer can effectively reduce various complications and improve overall survival[14]. Furthermore, the presence of liver metastases leads to the suppression of splenic dendritic cells, which poses a challenge to anti-tumor vaccination efforts. Measurement of spleen stiffness was the only predictor of late HCC recurrence and was directly related to the extent of liver disease and portal hypertension, both of which were associated with HCC recurrence[15]. According to a comment made on the article, it was proposed that splenic stiffness during HCC might be influenced to some extent by alterations in the immune system within the spleen[16]. Therefore, the spleen may play an irreplaceable role in immune surveillance of local invasion and metastasis in HCC.

Mouse iNKT is characterized by the expression of the unique CD1d-restricted T cell receptor (TCR) Vα14Jα18[17]. Interestingly, both the frequency and function of iNKTs in the tumor or circulation have been found to be highly correlated with overall survival in numerous malignancies[18–21]. For instance, iNKT can inhibit the growth of murine HCC by improving oncogenic beta-catenin-induced chronic inflammation in the liver[22,23]. Methylcholanthrene (MCA) was shown to initiate spontaneous tumor growth more rapidly in *Ja18*$^{-/-}$ mice (iNKT-deficient) in comparison to the wild-type mice, and isolated iNKTs were found to display direct cytotoxicity against MCA-induced sarcoma[24]. Disruption of commensal gut bacteria in mice can induce hepatic iNKT-mediated anti-tumor effects[25]. Adoptive transfer of autologous iNKTs has demonstrated promising safety and efficacy in treating advanced HCC[26,27]. Concurrently, iNKT-induced anti-tumor effects have been reported to be pleiotropic, such as TCR-engineered iNKTs can induce potent anti-tumor responses by dual targeting of both cancer and suppressive myeloid cells[28]. Moreover, in all the above- described studies, iNKTs have demonstrated direct and/or indirect anti-tumor immune surveillance effects. Nevertheless, the precise role of splenic iNKT, particularly in relation to local invasion of HCC, remains predominantly unrevealed.

Here, the findings highlight the distinctive function of splenic iNKTs in controlling immune surveillance in the context of local invasion of HCC. The interferon-γ (IFN-γ)/IFN-γR-dependent interaction between iNKT and CD4$^+$ T cells can promote the migration of CD4$^+$ T cells from the marginal zone into the white pulp, a key event in preventing local intrahepatic invasion of HCC. This study provides insights into understanding of how splenic iNKT drives immune surveillance of local invasion of tumor cells and facilitate the development of iNKT cell-based anti-cancer immunotherapies.

## Results

### Splenic iNKT deficiency exacerbates metastasis of hepatocellular carcinoma

To validate the potential role of splenic iNKT in hepatocellular carcinoma metastasis, we established a mouse model of intrahepatic metastasis of hepatocellular carcinoma (HCC-m) mouse model. $5 \times 10^5$ Hepa1-6 cells were injected orthotopically into the mouse liver and the liver tissues at the injection site were subsequently removed. After 2 weeks, Hepa1-6 cells in the circulation were found to recolonize in the liver parenchyma to form intrahepatic metastases. In addition, compared with the control mice, the spleen volume as well as weight of HCC-m the mice were significantly increased (Fig. 1A). Splenectomized mice displayed more severe HCC metastasis, with a significant increase in the tumor weight (Fig. 1B). To gain a deeper understanding of how the spleen can suppress HCC metastasis, we analyzed both the percentages and absolute numbers of the different immune cell populations in the spleens of HCC-m mice at 2 weeks. We identified that both the percentage and absolute number of splenic iNKTs were significantly elevated in HCC-m mice at 2 weeks (Fig. 1C–E). We observed that the percentage and absolute number of splenic CD4$^+$ T cells decreased, whereas the percentage of splenic CD8$^+$ T cells increased in HCC-m mice (Fig. 1F–H). However, there were no significant differences noted in the percentages and absolute numbers of splenic B cells and NK cells among these two groups of mice (Fig. S1A–F). We further examined the possible effect of iNKT on HCC metastases in *Ja18*$^{-/-}$ mice, HCC-m models for wild-type (WT) and *Ja18*$^{-/-}$ mice were constructed and tumor weights were analyzed after 2 weeks. Interestingly, iNKT deficiency significantly aggravated the HCC metastasis, but adoptive transfer of iNKT in the spleen effectively inhibited this process (Fig. 1I, J). These findings confirmed that splenic iNKTs have the ability to inhibit HCC metastasis.

### The presence of iNKT contributes to the maintenance and activation of CD4$^+$ T cells

We performed additional experiments to provide a clearer understanding of the crucial role played by iNKTs - which make up only about 2% of non-parenchymal cells in the spleen - in suppressing HCC metastasis. iNKT serves as a bridge between innate immunity and adaptive immunity and plays a crucial role in the initial stage of the disease[29]. Therefore, we focused towards determining whether impairments in iNKTs have any impact on immune cell populations 3 days after injection of Hepa1-6 cells. We thus analyzed the differences in the percentages of the major immune cell populations in the spleen of *Ja18*$^{-/-}$ mice. We observed that at steady state, *Ja18*$^{-/-}$ mice exhibited decreased basal CD4$^+$ T cell number in comparison to the control mice (Fig. 2A–C). The reduced number of splenic CD4$^+$ T cells caused by HCC metastasis was further worsened by iNKT deficiency, resulting in a further decrease in both the number and percentage of CD4$^+$ T cells (Fig. 2A–C). However, iNKT deficiency had no impact on the percentages of splenic B cells (Fig. S2A, B) and NK cells (Fig. S2C, D). Adoptive transfer of iNKTs to the spleen can effectively restore the reduction in splenic CD4$^+$ T cell percentage caused HCC metastasis (Fig. 2D, E). This observation led us to investigate whether iNKTs have the ability to promote the proliferation of CD4$^+$ T cells. Consistent with our expectations, splenic CD4$^+$ T cells from both *Ja18*$^{-/-}$ mice and *Ja18*$^{-/-}$ mice with HCC-m exhibited diminished proliferation ability, indicated by the low level of Ki67 expression (Fig. 2F, G). However, iNKT deficiency did not affect the apoptosis of CD4$^+$ T cell (Fig. S2E, F). The expression of CD1d is crucial for the cross-talk between antigen-presenting cells and iNKTs. We analyzed the expression levels of CD1d on CD4$^+$ T cells in the spleens of HCC-m and control mice by flow cytometry. Both groups of mice showed almost no expression of CD1d on splenic CD4$^+$ T cells (Fig. S2G, H). Similarly, splenic CD4 + T cells of iNKT-deficient mice also lacked expression of CD1d (Fig. S2G, H). In addition, the expression of the T cell activation marker CD69 and the level of interleukin-4 (IL-4) were both reduced in splenic CD4$^+$ T cells of *Ja18*$^{-/-}$ mice in comparison to the control mice (Fig. 2H, I). Interestingly, the expression levels of IFN-γ, IL-6 and TNF-α in CD4$^+$ T cells were not affected by iNKT deficiency (Fig. 2H, I). Therefore, the cross-talk between iNKT and CD4$^+$ T cells can play a vital role in inhibiting HCC metastasis.

### CD4$^+$ T cells in *Ja18*$^{-/-}$ mice exhibited unique mRNA expression patterns associated with impaired cell migration function

To investigate the impact of iNKT cell interactions with CD4$^+$ T cells on HCC metastasis in vivo, we isolated CD4$^+$ T cells from both WT HCC-m and *Ja18*$^{-/-}$ HCC-m mice and performed RNA sequencing analysis. Interestingly, 648 DEGs were identified in the splenic CD4$^+$ T cells of WT HCC-m and *Ja18*$^{-/-}$ HCC-m mice. Among them, 292 genes were found to be upregulated, whereas 356 genes were downregulated (*Ja18*$^{-/-}$ vs Ctrl, Fig. 3A). GO enrichment of the DEGs (*Ja18*$^{-/-}$ vs Ctrl, Down) was conducted in major functional classes of biological processes (BP), cellular components (CC), and molecular functions (MF). The downregulated DEGs were significantly annotated in the processing of T cell activation

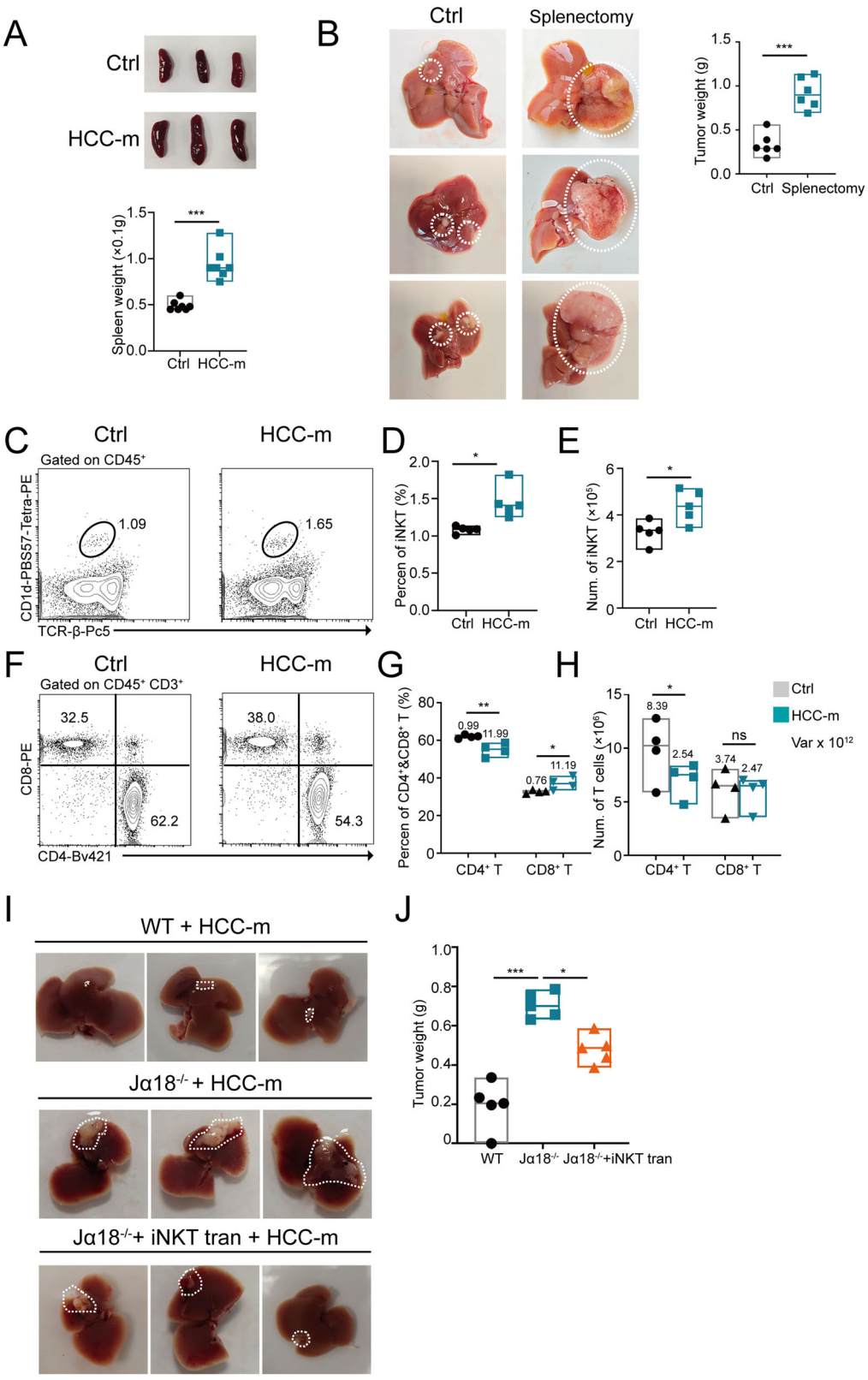


including protein phosphorylation, TCR V(D)J recombination, positive regulation of the TCR signaling pathway, as well as stress activated protein kinase signaling pathway (Fig. 3B). In addition, consistent with the previous descriptions, signaling pathways related to the cell cycle and cell proliferation were downregulated in $CD4^+$ T cells from *Ja18*$^{-/-}$ mice (Fig. 3B). Furthermore, downregulation of signaling pathways related to cytoskeleton organization and cell adhesion was also noted, thus suggesting changes in $CD4^+$ T cell motility in *Ja18*$^{-/-}$ mice (Fig. 3B). Annotation of the cellular components revealed that histone methyltransferase complex, cytoskeleton and TCR complex were also significantly downregulated (Fig. 3C). As for the molecular functions, the downregulated DEGs were significantly annotated for the transferase activity, protein binding, DNA binding,

**Fig. 1 | iNKT deficiency is beneficial for the metastasis of hepatocellular carcinoma. A** Representative appearance (left) and spleen weight (right) of spleens from the control mice and mice with metastasis ($n = 7$). **B** $5 \times 10^5$ Hepa1-6 cells were injected orthotopically into the mouse liver, and the liver tissues at the injection site was subsequently removed. The representative appearance of livers from the control and splenectomized mice (left) and tumor weight (right) ($n = 6$). **C** The proportion of the $CD45^+$ TCR-$\beta^+$ CD1d-PBS57-$Tetramer^+$ iNKT obtained from the spleens of control mice and mice with metastasis were analyzed using the flow cytometry. The isotype Ig of each antibody was used as a negative control. **D** Quantification of the percentage and **E** absolute number of iNKT in the indicated group ($n = 5$). **F** Flow cytometry analysis of the percentages of $CD45^+$ $CD3^+$ $CD4^+$ T cell and $CD45^+$ $CD3^+$ $CD8^+$ T cell in the spleens of control and HCC-m mice. **G** The percentage and **H** absolute number of $CD4^+$ T cells and $CD8^+$ T cells in both groups of mice were statistically analyzed. The variance has been marked on the graph ($n = 4$). **I** Representative appearance of the liver metastasis tumors in WT+Hepa1-6, $Ja18^{-/-}$+Hepa1-6 and $Ja18^{-/-}$+Hepa1-6+iNKT adoptively transferred mice. For the establishment of the splenic iNKT adoptive transfer mouse model, $5 \times 10^5$ iNKTs were orthotopically injected into the spleen of the recipient mouse. Tumor tissue is shown within the dotted box. **J** Statistical analysis of the liver tumor weights of mice in each group ($n = 5$).

histone methyltransferase activity (Fig. 3D). These molecules can promote the specific gene expression as well as regulate genome stability, cell maturation, DNA methylation, and cell mitosis. Moreover, the Kyoto encyclopedia of genes and genomes (KEGG) enrichment analysis indicated that the downregulated DEGs were associated with the processes such as cell growth and death, cell motility, amino acid metabolism, glycan biosynthesis as well as metabolism, which have been linked to the anti-tumor effect of T cells (Fig. 3E). Gene set variation analysis (GSEA) pathway enrichment analysis revealed that $CD4^+$ T cells in $Ja18^{-/-}$ mice were able to significantly down-regulate inflammatory response and cell surface receptor-related signaling pathways, thereby suggesting that their activation was effectively inhibited. Furthermore, $CD4^+$ T cells in $Ja18^{-/-}$ mice downregulated the various mRNA-encoding proteins associated with cell migration/chemotaxis functions, including cell adhesion, chemotaxis, leukocyte migration and lymphocyte chemotaxis (Fig. 3F).

Gene Ontology (GO) enrichment of the DEGs ($Ja18^{-/-}$ vs Ctrl, Up) was conducted in the GO categories of cellular component (CC), molecular function (MF), and biological process (BP). iNKT deficiency led to significant upregulation of DEG annotations in extracellular space, endothelial reticulum, chaperone complex, peroxidase activity, antioxidant activity, and cellular oxidation detoxification-related genes in $CD4^+$ T cells (Fig. S3A–C). In addition, protein processing in the endothelial reticulum, ferroptosis, and apoptosis-related pathways were significantly upregulated in the $CD4^+$ T cells of $Ja18^{-/-}$ mice, suggesting that iNKT cells play an important role in the function of $CD4^+$ T cells (Fig. S3D).

### HCC metastasis can promote the migration of splenic $CD4^+$ T cells from the marginal zone into the WP

To observe the behavioral pattern of $CD4^+$ T cells in HCC-m mice, we examined the distribution of iNKTs and $CD4^+$ T cells in the spleen of $CXCR6^{GFP/+}$ mice. We employed intravital microscopy to observe the behavior of iNKTs and $CD4^+$ T cells at two different time points (0 h and 4 h following orthotopic injection of Hepa1-6 cells into the liver). At steady state, $CD4^+$ T cells were found to colocalize with iNKTs in the marginal zone without entering the splenic WP (Fig. S4A). However, 4 h after injection of Hepa1-6 cells into the liver, $CD4^+$ T cells were observed to gradually entere the splenic WP (Fig. 4A, B). $CD4^+$ T cells in the splenic WP of HCC-m mice were also verified using Z-stack analysis (Fig. 4C, supplementary Video S1). To validate this finding, we next intravenously administered APC-conjugated anti-CD45 antibodies to identify $CD4^+$ T cells present in the marginal zone. We noticed that following injection of the Hepa1-6 cells, the proportion of $CD4^+$ T cells within the WP began to increase after 4 h, whereas the percentage of $CD4^+$ T cells in the marginal zone exhibited a significant decline (Fig. 4D, E). Furthermore, we also confirmed the characteristic changes in dynamics of splenic $CD4^+$ T cell during HCC metastasis (Fig. 4F). It was observed that in comparison to the the control group, the crawling distance as well as crawling velocity of splenic $CD4^+$ T cells in HCC-m mice were significantly increased, which facilitated their rapid entry into the WP (Fig. 4G, H). At the same time, HCC-m mice increased the number of contacts between splenic iNKT and $CD4^+$ T cells (Fig. 4I, supplementary Video S2). Simultaneously, iNKTs in HCC-m mice exhibited tight interactions with $CD4^+$ T cells, whereas there was no intercellular contact observed between iNKTs and $CD4^+$ T cells in the control mice (Fig. 4J, K).

### The entry of $CD4^+$ T cells into the WP depends on IFN-γ secreted by iNKT

To investigate the role of iNKTs in $CD4^+$ T cell migration, we initially examined the expression of iNKT cell activation markers and cytokines in the spleens of HCC-m mice and control mice. Splenic iNKT of HCC-m mice was found to significantly upregulate the expression of CD69, a well characterized marker of iNKT activation (Fig. S5A, B). Moreover, iNKT in HCC-m mice was able to significantly upregulate the expression levels of IFN-γ and TNF-α, while displaying no impact on the expression of IL-4 (Fig. 5A, B). Other types of immune cells such as NK cells, B cells, $CD4^+$ T cells, and macrophages do not express IFN-γ (Fig. S5C, D). Interestingly, $CD8^+$ T cells expressed a certain level of IFN-γ under homeostasis, whereas in HCC-m mice, $CD8^+$ T cells were no longer able to express IFN-γ (Fig. S5E, F). We also noticed that $CD4^+$ T cells highly expressed IFN-γ receptor α chain, but did not express TNFR I (Fig. 5C, D). In contrast to control mice, $CD4^+$ T cells from HCC-m mice exhibited increased expression of the IFN-γ receptor α chain (Fig. 5C, D). We further confirmed that NK cells can also express a certain level of IFN-γ α chain (Fig. S5G, H), but only 2-3% of the B cell population can express IFN-γ α chain (Fig. S5G, H), and $CD8^+$ T cells and macrophages were not found to express IFN-γ α chain (Fig. S5G, H). There was no difference observed in expression of IFN-γ α chain by NK cells and B cells between HCC-m mice and the control mice (Fig. S5G, H).

To investigate the potential relationship between iNKTs and $CD4^+$ T cells in the mouse spleen, we isolated WT and IFN-$\gamma^{-/-}$ mouse-derived iNKT cells and transferred them into the spleens of $Ja18^{-/-}$ mice. After establishing the HCC-M model, flow cytometry was used to analyze the proportion of splenic $CD4^+$ T cells entering the white pulp. We injected fluorescein-conjugated anti-CD45 antibodies into the circulatory system through the tail vein. The antibody is able to bind to $CD4^+$ T cells in the red pulp but is unable to contact $CD4^+$ T cells in the white pulp. It was found that IFN-γ-deficient iNKT cells did not allow entry of $CD4^+$ T cells into the white pulp in contrast to WT-iNKT (Fig. 5E, F). Further, we orthotopically injected Hepa1-6 cells into $Ja18^{-/-}$ mice and subsequently analyzed the behavior of $CD4^+$ T cells in the spleen. After 4 h of injection of Hepa1-6 cells, iNKT deficiency caused a significant decrease in the number of $CD4^+$ T cells entering into the WP (Fig. 5G, H). Moreover, $CD4^+$ T cell entry into the WP was also inhibited in the spleens of $CXCR6^{GFP/+}$ IFN-$\gamma^{-/-}$ mice (Fig. 5G, H). iNKT deficiency also contributed to reduced expression of *Stat*1 in $CD4^+$ T cells, which is a key transcription factors in IFN-γ signaling pathway (Fig. 5I). iNKT deficiency also caused a substantial decrease in the mRNA level of CD40L in $CD4^+$ T cells (Fig. 5J), which can interact with CD86 on the surface of B cells to mediate the activation of B cell. We further analyzed the protein levels of STAT1 phospho and CD40L on $CD4^+$ T cells in the spleens of $Ja18^{-/-}$-HCC-m and WT-HCC-m mice using flow cytometry. As expected, $Ja18^{-/-}$ mice showed lower protein levels of STAT1 phospho and CD40L on $CD4^+$ T cells compared to the WT mice (Fig. S5I, J). IFN-γ deficiency also significantly reduced expression of IL-4 by $CD4^+$ T cells (Fig. 5K, L), which has been reported to be crucial for both the survival

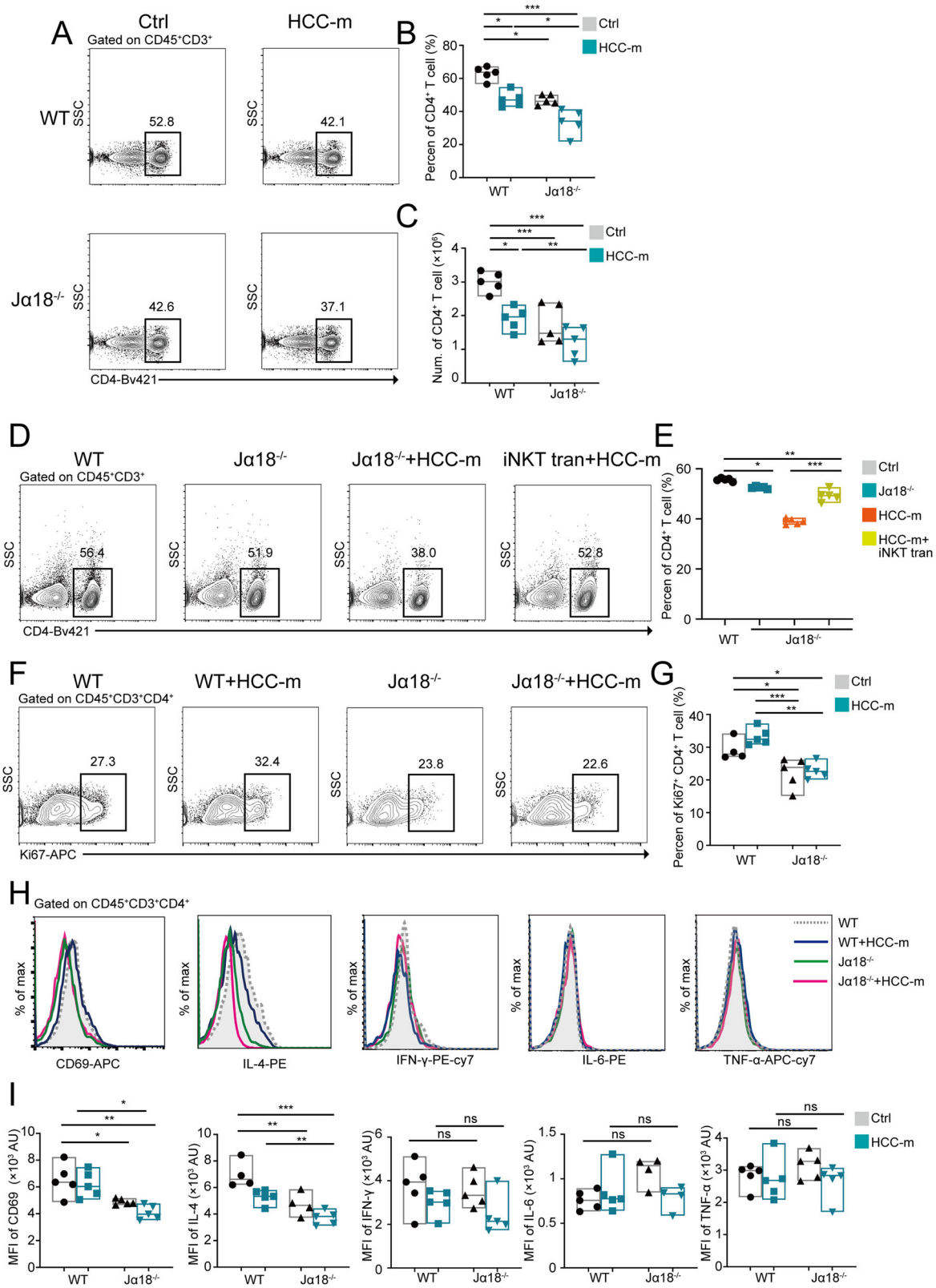


**Fig. 2 | The cross-talk between iNKT and CD4$^+$ T cells helps to control the metastasis of hepatocellular carcinoma.** **A** Proportion of the CD45$^+$ CD3$^+$ CD4$^+$ T cells derived from the spleens of WT mice, WT mice with HCC metastasis, *Jα18*$^{-/-}$ mice and *Jα18*$^{-/-}$ mice with metastasis were analyzed using flow cytometry. **B** Quantification of the percentage and **C** absolute number of CD4$^+$ T cell in the indicated group. **D** Proportion of the CD4$^+$ T cells obtained from the spleens of WT mice, *Jα18*$^{-/-}$ mice, *Jα18*$^{-/-}$ mice with HCC metastasis and *Jα18*$^{-/-}$+Hepa1-6+iNKT adoptively transferred mice were analyzed using flow cytometry. **E** Quantification of the percentage of CD4$^+$ T cell in the indicated group. **F** Flow cytometry analysis of the percentage of Ki67$^+$ CD4$^+$ T cell in WT, WT + HCC-m, Jα18$^{-/-}$, Jα18$^{-/-}$ + HCC-m mice. **G** Statistical analysis of the percentage of Ki67$^+$ CD4$^+$ T cell in each group. **H** Analysis of CD69, IL-4, IFN-γ, IL-6, and TNF-α in CD4$^+$ T cells of the indicated group through flow cytometry. **I** Statistical analysis of CD69, IL-4, IFN-γ, IL-6, and TNF-α mean fluorescence intensity (MFI) of CD4$^+$ T cells of the indicated group ($n = 5$). The data shown was obtained from three independent experiments with $n = 5$ mice per group. The data has been displayed as the mean ± SEM. $^*P < 0.05$, $^{**}P < 0.01$, $^{***}P < 0.001$.

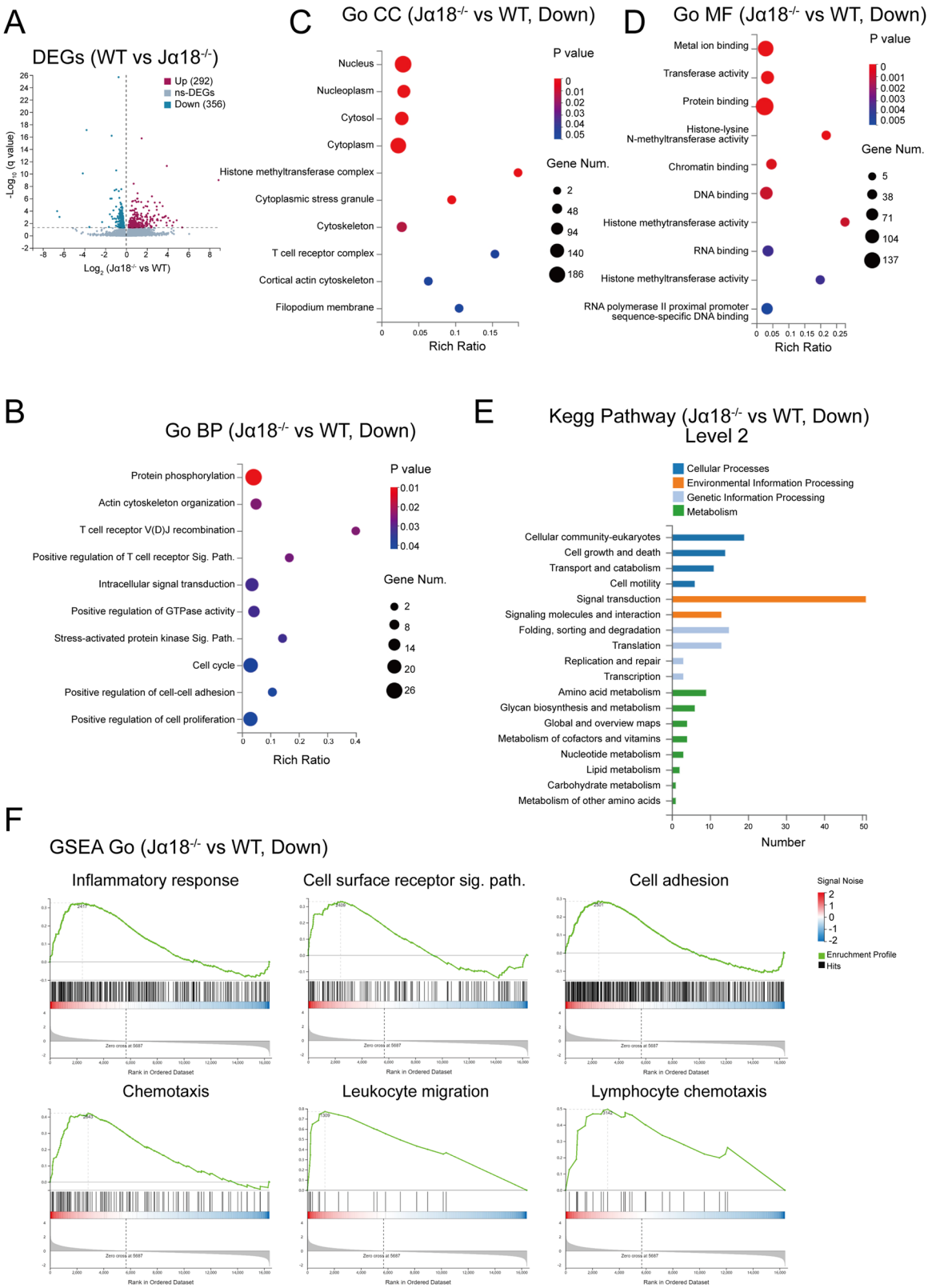


**Fig. 3 | Transcriptional characteristics of splenic CD4$^+$ T cells in iNKT-deficient HCC-m mice. A** Volcano map depicting DEGs in CD4$^+$ T cells from WT+Hepa1-6 and *Jα18*$^{-/-}$+Hepa1-6 mice. Each group contained 3 mice. **B** GO enrichment of the various downregulated genes (*Jα18*$^{-/-}$ mice vs WT mice) in the biological processes, **C** cellular components, and **D** molecular functions. **E** KEGG enrichment analysis of the different downregulated genes. **F** Gene set enrichment analysis of the various downregulated genes.

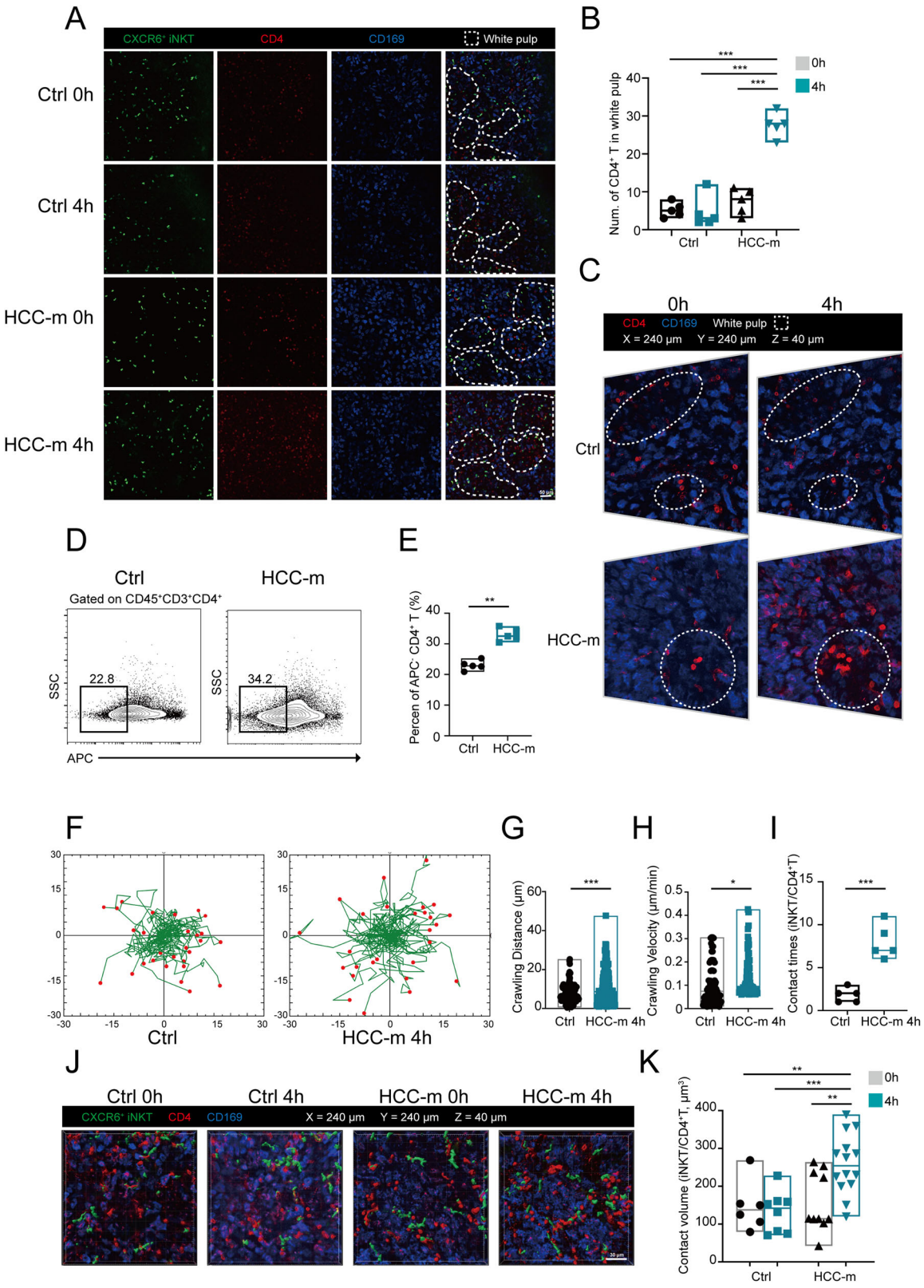


and function of B cells. Therefore, it was concluded that in HCC-m mice, IL-4 secretion by $CD4^+$ T cells depends primarily on the IFN-γ signal provided by iNKTs. However, IFN-γ deficiency did not affect the expression of CD86 on B cells (Fig. S5K, L). Collectively, these results highlighted the pivotal role of IFN-γ signaling pathway in regulating the migration of $CD4^+$ T cells into the WP.

### Splenic $CD4^+$ T cell depletion leads to increased metastatic burden of hepatocellular carcinoma

To clarify whether $CD4^+$ T cells contribute to the inhibition of HCC metastasis, we injected a $CD4^+$ T cell-depletion antibody in situ into the mouse spleens (50 μg/3 days, a total of 7 injections). Subsequent flow cytometry analysis indicated depletion of ~80% of splenic $CD4^+$ T cells

**Fig. 4 | Splenic CD4$^+$ T cells in mice with HCC-m enhanced their interaction with iNKT and subsequently facilitated migration into the white pulp. A** Intravital microscopic observation of the spleen was carried out 4 h after the Hepa1-6 cell was injected orthotopically into the spleen of CXCR6$^{Gfp/+}$ mice. Fluorescein-conjugated anti-mouse CD4 and CD169 antibodies were employed to label CD4$^+$ T cells (Red) and marginal zones (Blue). Scale bar, 100 μm. White pulps have been indicated with a white dashed line. **B** Statistical analysis of the number of CD4$^+$ T cells in white pulp in each group. **C** Representative Z-Stack fluorescence co-localization images (X = 240 μm, Y = 240 μm, Z = 40 μm) were obtained to analyze the potential interactions between CD4$^+$ T cells and white pulp at the different time points. **D** Flow cytometry analysis of the proportion of CD4 + T cells in the spleen white pulp of mice with HCC metastasis. Anti-mouse CD45-APC antibody was injected into the tail vein of the mice 1 h before the experiment. APC$^-$ CD4$^+$ T cells were CD4$^+$ T cells located in the white pulp. **E** Statistical analysis of the percentage of CD4$^+$ T cell in the white pulp. **F** Determination of the migration trajectories of CD4$^+$ T cells in the control and HCC-m mice after adjusting the starting position. The data was collected from 5 mice, and scanned for 10 min at 2-s intervals. A red dot represents one CD4$^+$ T cell. **G** Statistical analysis of the crawling distance and **H** crawling velocity of mouse splenic CD4$^+$ T cells 4 h after orthotopic injection of Hepa1-6 cells into the liver. **I** Statistical analysis of the number of contacts formed between splenic iNKT and CD4$^+$ T cells within 10 min. **J** Representative Z-Stack fluorescence co-localization images (X = 240 μm, Y = 240 μm, Z = 40 μm) were collected to examine the potential interactions between CD4$^+$ T cells and iNKTs in different time points. **K** Statistical analysis of the contact volume between CD4$^+$ T cells and iNKT in each group. The data shown was obtained from three independent experiments with $n = 5$ mice per group. The data has been displayed as the mean ± SEM. $^*P < 0.05$, $^{**}P < 0.01$, $^{***}P < 0.001$.

(Fig. 6A, B). Splenic CD4$^+$ T cell depletion exacerbates intrahepatic metastasis of hepatocellular carcinoma (Fig. 6C, D). Furthermore, depletion of splenic CD4$^+$ T cells in *Jα18*$^{-/-}$ mice led to more severe hepatocellular carcinoma metastasis (Fig. 6C, D).

### CD4$^+$ T cells regulate splenic B cells from HCC-m mice migrate to the liver and exert cytotoxic effects on Hepa1-6 cells

First, 100 μl of EZ-Link Sulfo-NHS-LC-Biotin was injected in situ into the spleens of Ctrl and HCC-m mice. This biotinylates only surface proteins of whole cells as the negatively charged reagent does not permeate cell membranes. The biotin on the surfaces of spleen-derived cells was able to bind to fluorescein-conjugated streptavidin but not to liver-derived cells. Only 5% of the splenic CD4$^+$ T cells migrated to the liver in both WT and HCC-m mice (Fig. S6A, B) and there was no statistical difference between the two groups. Similarly, splenic CD8$^+$ T and iNKT cells showed minimal migration to the liver (Fig. S6C–F). To verify whether CD4$^+$T cells exhibited cytotoxicity toward Hepa1-6 cells, we purified CD4$^+$T cells from the spleens of WT and HCC-m mice and co-cultured them with Hepa1-6 cells. We used Zombie UV™ dye to analyze the mortality rate of Hepa1-6 cells. Zombie UV™ is an amine reactive fluorescent dye that does not penetrate live cells but is taken up by cells with compromised membranes. Thus, it can be used to assess the live vs. dead status of mammalian cells. The use of the dye showed that CD4$^+$T cells from both groups of mice had no direct cytotoxic effects on Hepa1-6 cells (Fig. S6G, H). Meanwhile, the expression of CD69, an activation marker, is upregulated by hepatic CD4$^+$ T cells in HCC-m mice (Fig. S6I, J). Although hepatic CD4$^+$ T cells showed basal expression of IL-4, no difference in expression was found between HCC-m and Ctrl mice (Fig. S6I, J). Furthermore, hepatic CD4$^+$ T cells did not express either IFN-γ or CD40L (Fig. S6I, J).

Surprisingly, a portion of splenic B cells were observed to migrate to the liver, and this proportion was significantly higher in HCC-m mice compared to the WT controls (Fig. 7A, B). The depletion of CD4$^+$T cells significantly reduced the directed migration of splenic B cells to the liver (Fig. 7A, B), suggesting that CD4$^+$ T cells are critical for the resistance of splenic B cells to intrahepatic metastasis of hepatocellular carcinoma. Meanwhile, the frequency of hepatic B cells was significantly increased in HCC-m mice compared with control mice, and the depletion of CD4$^+$ T cells resulted in a significant decrease in the frequency of hepatic B cells (Fig. 7C, D). Co-culture of splenic B cells derived from HCC-m mice and Hepa1-6 cells resulted in a significant increase in the rate of apoptosis in the latter (Fig. 7E, F). However, splenic B cells derived from control mice did not exhibit cytotoxicity against Hepa1-6 cells, strongly suggesting a significant role for CD4$^+$ T cells in B cell resistance to Hepa1-6 cells (Fig. 7E, F). Additionally, spleen-derived B cells expressed higher levels of IgM compared to B cells originating from the liver, suggesting a stronger anti-tumor effect (Fig. 7G, H). In conclusion, although CD4$^+$ T cells were unable to migrate from the spleen to the liver in large numbers, they could regulate the migration of splenic B cells to the liver and were able to kill HCC cells through upregulation of the expression of IgM. In addition, we observed a significant reduction in CD40, MHC-II, and IgM expression in splenic B cells from *Jα18*$^{-/-}$ mice (Fig. 7I, J). These data confirm that B cell activation is closely associated with the anti-metastatic cascade orchestrated by iNKT and CD4$^+$ T cells.

## Discussion

Herein, we present evidence that the interaction between splenic iNKT and CD4$^+$ T cells plays a key role in inhibition of HCC metastasis. Splenectomy and iNKT deficiency both can exacerbate the metastasis, but splenic iNKT cell adoption can significantly decrease the burden of HCC metastasis. Further analysis of the phenotypic changes of CD4$^+$ T cells in HCC metastasis model of *Jα18*$^{-/-}$ mouse revealed key differences between CD4$^+$ T cells and other immune cell populations. These findings indicate that iNKT can interact with CD4$^+$ T cells in the subtissue niche of the spleen and affect the secretion of IL-4 by the latter. RNA-seq analysis revealed the impact of iNKT deficiency on the transcriptional signature of CD4$^+$ T cells, which can significantly impair the migration of CD4$^+$ T cells. iNKT and CD4$^+$ T cells are mainly co-localized in the spleen marginal zone, and IFN-γ can serve as an important factor in regulating the entry of CD4$^+$ T cells into the WP. Subsequently, splenic B cells migrate to the liver and exert cytotoxic effects on Hepa1-6 cells. Collectively, these results demonstrated that the cross-talk between iNKT and CD4$^+$ T cells was a critical event in mediating immune signaling between the splenic marginal zone and WP, ultimately impacting the progression of local invasion in HCC.

In advanced tumors, both tumor-specific CD4$^+$ and CD8$^+$ T cells lack effector functions and express inhibitory receptors. This dysfunction/exhaustion could be primarily attributed to continued exposure (for days to weeks) to various tumor antigens and the immunosuppressive tumor microenvironment[30–32]. During acute infection, 24 h of antigen stimulation was found to be sufficient to facilitate CD8$^+$ T cell proliferation and differentiation into functional effector and memory states[33,34]. In addition, recent studies have also reported that the function of CD8$^+$ T cells in tumor-bearing hosts was severely impaired 12 h after exposure to the tumor antigens, and this reduction in effector function can begin as early as 6 h[35]. Therefore, the initial 12 h after antigen exposure can serve as a critical window for determining T cell fate and anti-tumor effects.

iNKT plays a crucial role in mediating CD4$^+$ T infiltration into the WP and IL-4 secretion, which is important for subsequent B cell-associated anti-tumor effects. Activated B cells can proliferate and eventually differentiate into three distinct functional subpopulations: germinal center B cells (GC B cells) which undergo affinity maturation of their BCRs, thus ultimately producing the progeny cells with high affinity for the corresponding antigens, antibody-secreting B cells (ASCs) and memory B cells (MBCs)[36]. The characteristic somatic hypermutations and relaxed cell cycle checkpoint properties of GC B cells increase their susceptibility for the generation of self-reactive clones and thereby predispose them to apoptosis as a protective mechanism[37]. IL-4, (also known as B cell stimulation factor 1) has a significant impact on regulating almost every stage of B cell fate. IL-4 can effectively stimulate GC B cells by activating the BCL-XL—Stat6 axis while protecting them from apoptosis[38,39]. In addition, IL-4 as also possess the

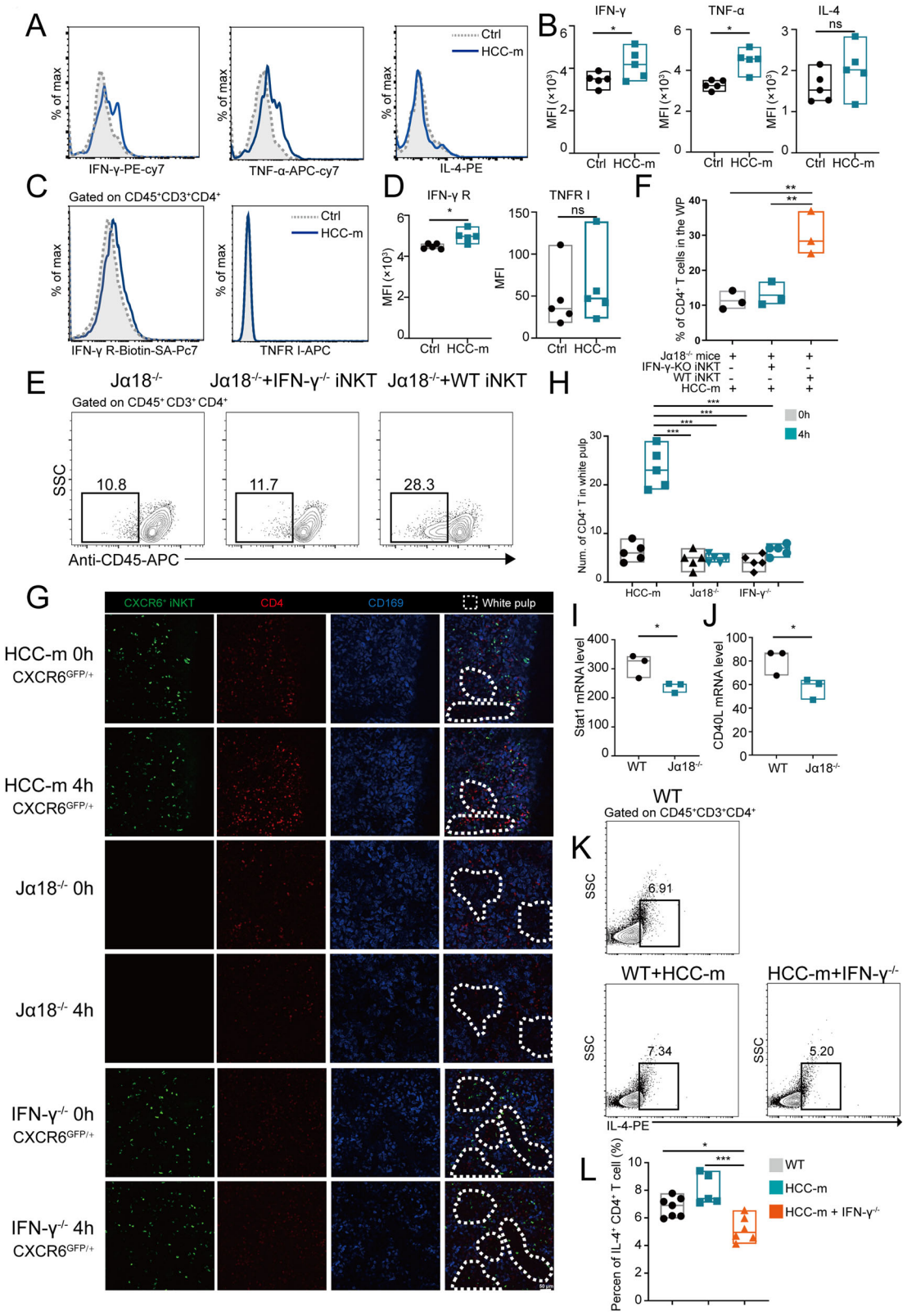


capability to function as a potential costimulatory cytokine to induce B cell proliferation[40]. Exposure of CD40L-stimulated B cells to IL-4 can promote their polarization towards antigen-presenting cells[41]. Although IL-4 is not required for antibody formation, it can serve as an important driver of IgE and IgG1 class switching and can thereby promote the differentiation of B effector 2 cells[42,43]. Moreover, IL-4 can profoundly influence the differentiation fate of B cells by promoting differentiation of MBC and negatively regulating the fate of ASC[44].

Although immuno-oncology remains T-cell centric, several recent studies concur that B-cell-infiltrated tumors have significantly better prognosis and enhanced T-cell responses. The focus has been on the B cells' capacity to cross present antigens to T cells when discussing their role in

**Fig. 5 | The migration of CD4$^+$ T cells into the spleen white pulp was primarily dependent on the IFN-γ/IFN-γ receptor signaling pathway. A** Investigation of IFN-γ, TNF-α, and IL-4 in iNKTs of indicated group through flow cytometry. **B** Statistical analysis of IFN-γ, TNF-α, and IL-4 MFI of iNKTs of indicated group. **C** Determination of expression of IFN-γ receptor and TNFR I in CD4$^+$ T cells of indicated group through flow cytometry. **D** Statistical analysis of IFN-γ receptor and TNFR I MFI of CD4$^+$ T cells of the indicated group. **E** We periplasmically transferred primary iNKT cells ($1 \times 10^5$) derived from WT or IFN-γ$^{-/-}$ mice into the spleens of *Ja18*$^{-/-}$ mice, followed by establishment of the HCC-M mouse model. Three days later, the fluorescein-conjugated anti-mouse CD45 antibody was injected into the mouse tail veins 15 min before the mice were euthanized. CD4$^+$ T cells in the red pulp were able to bind to the antibody, while CD4$^+$ T cells in the white pulp were unable to bind to the antibody. Flow cytometry was performed to analyze the proportion of CD4$^+$ T cells located in the white and red pulp. **F** Statistical analysis of (**E**). **G** Intravital microscopic observation of the spleen was performed 4 h after Hepa1-6 cell were injected orthotopically into the spleen of CXCR6$^{Gfp/+}$, *Jα18*$^{-/-}$ and CXCR6$^{Gfp/+}$ IFN-γ$^{-/-}$ mice. Fluorescein-conjugated anti-mouse CD4 and CD169 antibodies were then used to label CD4$^+$ T cells (Red) and marginal zones (Blue). Scale bar, 100 μm. White pulps have been indicated with a white dashed line. **H** Statistical analysis of the number of CD4$^+$ T cells in white pulp in indicated group. **I** Expression levels of Stat1 and **J** CD40L mRNA in CD4$^+$ T cells of *Jα18*$^{-/-}$ mice and WT mice with HCC metastasis. **K** Flow cytometry analysis of expression levels of IL-4 in CD4$^+$ T cells of HCC-m IFN-γ$^{-/-}$ mice. **L** Statistical analysis of the percentage of IL-4$^+$ CD4$^+$ T cells in the indicated group. The data shown was obtained three independent experiments with $n = 5$ mice per group. The data has been displayed as the mean ± SEM. $^*P < 0.05$, $^{**}P < 0.01$, $^{***}P < 0.001$.

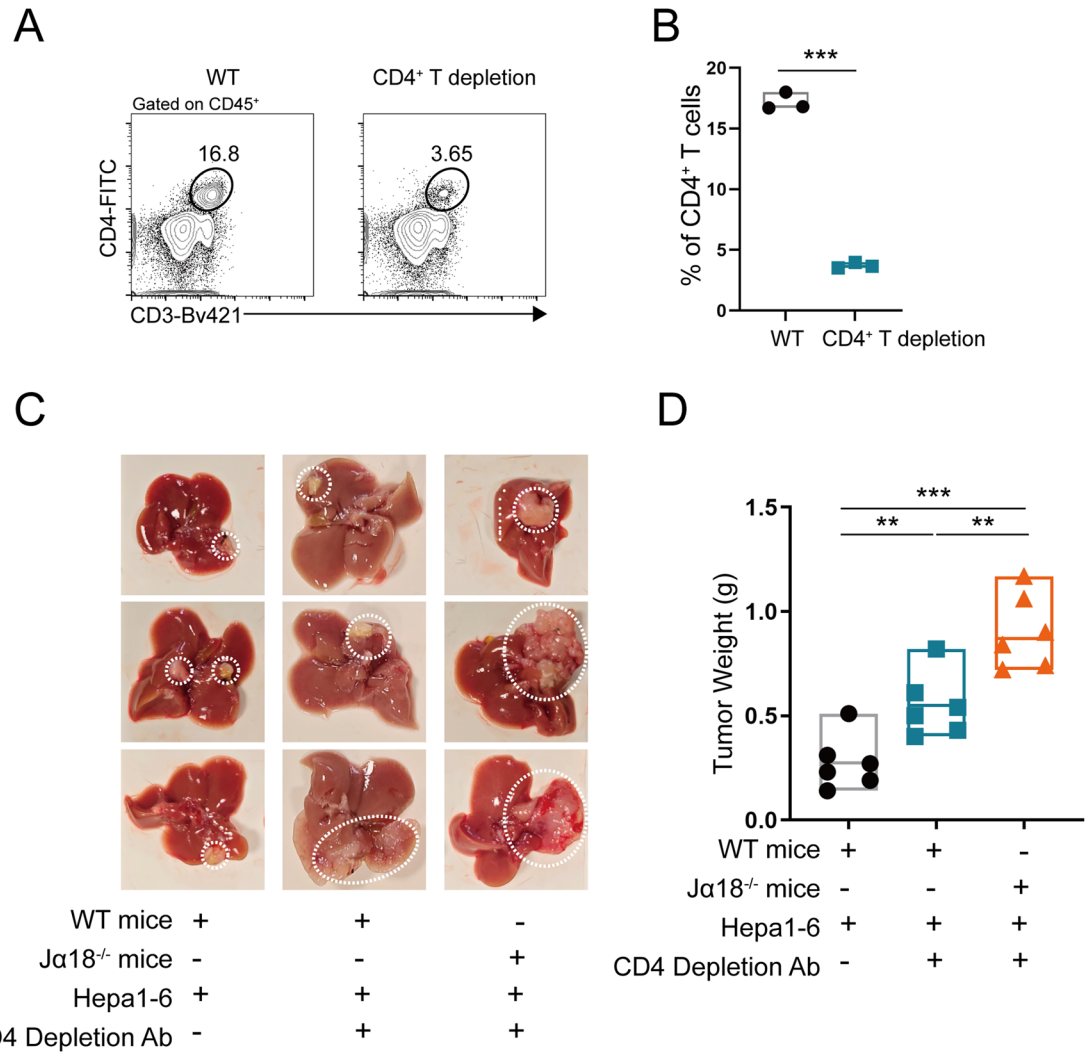


**Fig. 6 | Splenic CD4$^+$ T cell depletion leads to increased metastatic burden of hepatocellular carcinoma. A** Flow cytometry analysis of the proportion of splenic CD4$^+$ T cells in WT and CD4$^+$ T cell-depletion antibody intrasplenically injected mice. **B** Statistical analysis of (**A**) ($n = 3$). **C** Representative appearance of metastatic liver tumors in WT + Hepa1-6, WT + Hepa1-6 + CD4$^+$ T cell depletion antibody, and Jα18$^{-/-}$ + Hepa1-6 + CD4$^+$ T cell depletion-antibody mice. Tumor tissue is shown within the dotted boxes. **D** Statistical analysis of (**C**) ($n = 6$), $^{***}P < 0.001$. $^{**}P < 0.01$.

enhancing anti-tumor immunity. These B cells are usually organized into the tertiary lymphoid structures (TLS) and distributed inside or outside the tumor, which are predominantly aggregates of immune cells with lymph node-like characteristics that have been reported to generate both local and sustained immune responses[45,46]. B cells in TLS can form germinal centers and actively produce different antibodies that can potentially recognize tumor-associated antigens[47]. Antibodies secreted by B cells can effectively recognize extracellular domains present on the surface of tumor cells and thereby redirect the cytotoxic activity of both the natural killer cells and myeloid cells against the tumor cells[47]. Interestingly, antibodies also have the potential to facilitate uptake of the dying tumor cells by antigen-presenting cells, thereby exposing intracellular antigens through antigen presentation[48]. In addition, tumor cell-derived exosomes can also be effectively neutralized by antibodies[49]. Moreover, cytokine production by B cells can create a

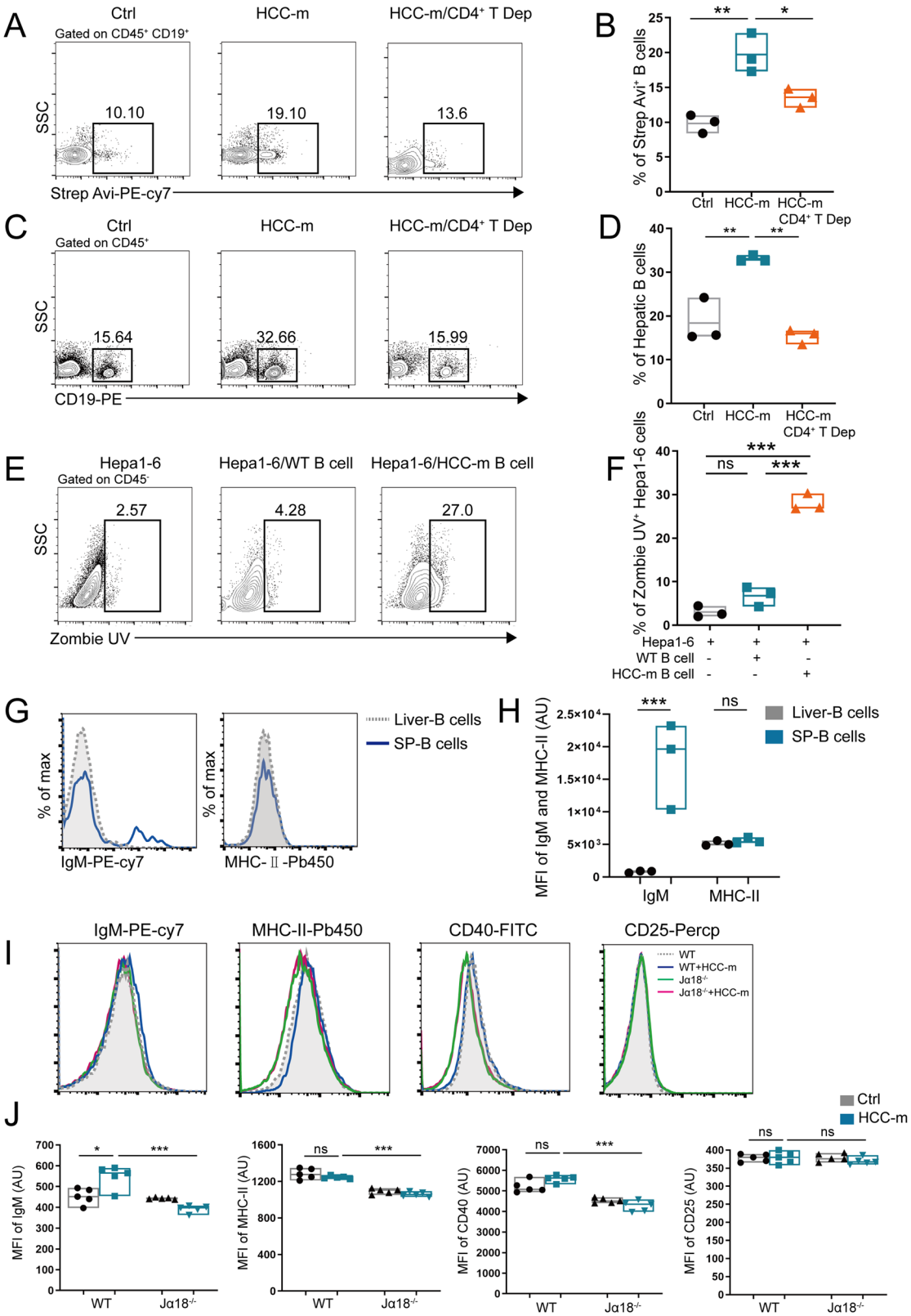


**Fig. 7 | Splenic B cells from HCC-m mice migrate to the liver and exert cytotoxic effects on Hepa1-6 cells. A** Flow cytometry was performed to analyze the percentage of spleen-derived B cells in the hepatic B cell pool in the Ctrl, HCC-m, and HCC-m/CD4$^+$ T cell-depleted groups. **B** Statistical analysis of (**A**). **C** Flow cytometry was used to analyze the frequency of hepatic CD19$^+$ B cells in control mice, HCC-m mice, and CD4$^+$ T cell depletion HCC-m mice. **D** Statistical analysis of (**C**). **E** Hepa1-6 cells ($5 \times 10^4$) were co-cultured with splenic B cells ($2 \times 10^4$) from WT or HCC-m mice in U-bottomed 96-well plates. After 3 days, the Hepa1-6 cells were collected and incubated with Zombie UV$^{TM}$ dye. The percentage of dead Hepa1-6 cells was analyzed by flow cytometry. **F** Statistical analysis of (**E**). **G** Flow cytometry was used to analyze the expression levels of IgM and MHC-II in liver-derived and spleen-derived B cells. **H** Statistical analysis of (**G**). **I** Flow cytometry was used to analyze the expression levels of IgM, MHC-II, CD40, and CD25 in B cells in WT and *Jα18*$^{-/-}$ mice. **J** Statistical analysis of (**I**). The data shown was obtained three independent experiments with $n = 3$ mice per group. The data has been displayed as the mean ± SEM. ***$P < 0.001$. **$P < 0.01$, *$P < 0.05$. NS: non-significant.

microenvironment that could be more permissive to effector T cells but detrimental to the tumor growth[50]. These properties of B cells can enable them to exert substantial anti-tumor effects even outside the tumor tissues, which is consistent with our current observations.

Our data reveal that splenic B cells, but not hepatic B cells, play a critical role in resisting local invasion of hepatocellular carcinoma. On the one hand, the spleen has a larger pool of B cells compared to the liver, where hepatic B cells represent only a small fraction of the intrahepatic immune cell population. In addition, B cells need to be activated in secondary lymphoid organs, such as the spleen and lymph nodes[51]. Hepatic B cells are predominantly B-2 cells and are characterized by the secretion of IgG-type antibodies. A specialized subpopulation of B cells exists at the margins of the splenic white pulp, termed marginal zone B cells (Mz-B cells). Mz-B cells are the main source of preexisting IgM in the body, and are capable of reacting to antigens and converting into IgM-secreting plasma cells[52]. IgM has a greater ability to activate the complement system compared to IgG, which in turn exerts a cytotoxic effect on target cells[53]. Therefore, splenic B cells have a stronger anti-tumor immune effect compared to hepatic B cells.

Overall, our current study proposes a mechanism through which the potential interaction of splenic iNKT and $CD4^+$ T cells can significantly limit metastasis of HCC by inducing B cell migration to the liver. $CD4^+$ T cells are primarily responsible for transmitting immune signals between the spleen marginal zone and the WP. Additional research is required to establish how B cells can effectively clear circulating tumor cells, consequently mitigating the development of liver metastases Therefore, it is anticipated that therapeutic approaches involving the activation of splenic iNKTs or adoptive transfer of iNKT to the spleen can effectively suppress the metastasis and recurrence of HCC after surgery.

## Conclusion

The findings of this study demonstrated that splenic iNKTs inhibit intrahepatic metastasis of hepatocellular carcinoma. Splenic iNKTs promote the entry of $CD4^+$ T cells into the white pulp through the secretion of IFN-γ. Subsequently, $CD4^+$ T cells modulated the migration of splenic B cells to the liver where they exert cytotoxic effects on Hepa1-6 cells. These findings demonstrating the successful inhibition of HCC metastasis by splenic iNKTs are of great significance. These results expand the understanding of the immune surveillance mechanism of iNKT-mediated metastasis.

## Methods

### Animal experiments

All mice were kept in a pathogen-free facility with a 12 h light/dark cycle and provided ad libitum access to food and water. All animal experiments were conducted according to protocols approved by the Animal Ethics Committee of the affiliated Suzhou Hospital of Nanjing Medical University (Project number K-2024-047). We have complied with all relevant ethical regulations for animal use. Eight-week-old wild-type C57BL/6 mice were purchased from ZiYuan Biotechnology Co. Ltd. (Hangzhou, China). The IFN-$\gamma^{-/-}$ mice were kindly provided by Professor Yuanli Chen (Hefei University of Technology, Hefei, China). In contrast to other groups who have shown that intrasplenic injection of Hepa1-6 cells leads only to the development of liver tumors[54], the present study established a mouse model of direct intrahepatic HCC metastasis to better simulate the process of HCC metastasis. This model was established by the direct orthotropic injection of $5 \times 10^5$ Hepa1-6 cells (obtained from the National Collection of Authenticated Cell Cultures of China) into the lower left lobe of the liver. After 10 min, two-thirds of the liver lobe was removed to ensure that the Hepa1-6 cells had entered the liver sinusoids but not the liver parenchyma (Fig. S7A). Control mice were treated with in situ injection of physiological saline into the liver, after which the liver tissue at the injection site was excised. The absolute number of $mCherry^+$ Hepa1-6 cells within the resected liver tissue was analyzed using flow cytometry. The data showed that the resected liver tissue contained approximately one-third of the Hepa1-6 cells, indicating that approximately two-thirds of the Hepa1-6 cells remained within the mouse liver tissue (Fig. S7B). After a specified time, the mice were sacrificed for further evaluation. In the mouse splenectomy model, a 2–3 mm incision was made in the back of the mouse, after which the spleen was ligated and excised directly, while in the control mice only the skin was incised but the spleen was not removed.

### Enrichment of murine splenic iNKTs and B cells

Single-cell suspensions of spleen cells were prepared as previously described[55]. For splenic iNKT or B cell enrichment, $5 \times 10^6$ splenocytes were collected and incubated with allophycocyanin (APC)-conjugated CD1d-PBS57-tetramer or an APC-conjugated anti-mouse CD19 antibody for 30 min at 4 °C in the dark. The iNKTs and B cells were thereafter isolated using an EasySep™ Mouse APC Positive Selection kit (Stem Cell, CA, USA). The purity of the cells after enrichment was over 95% (Fig. S7C). For the establishment of the splenic iNKT adoptive transfer mouse model, $5 \times 10^5$ iNKTs were injected orthotopically into the spleens of the recipient mice.

To analyze the distribution of iNKTs after adoptive transfer, $1 \times 10^5$ primary iNKT cells were injected in situ into the spleens of *Ja18*$^{-/-}$ mice. The mice were sacrificed three days later, and the absolute number of iNKT cells in the spleens, livers, and peripheral blood was analyzed by flow cytometry. The iNKTs in the spleen, liver, and peripheral blood accounted for ~61% of the total iNKT cell population (~$6.1 \times 10^4$ cells) (Fig. S7D). Additional cells may have been lost due to a variety of factors, such as cell death, lung sequestration, or random error, among others. Secondly, the spleen contained the greatest number of iNKT cells, accounting for ~85% of the total (Spleen + Liver + Blood = 100%) (Fig. S7E). The spleen retained the vast majority of iNKT cells in our iNKT cell adoption transfer model.

### Intravital microscopy

$CXCR6^{GFP/+}$ mice (Most iNKT cells express CXCR6, ~76% of $GFP^+$ cells were iNKTs (Fig. S7F)) were anesthetized by intravenous injection with 4 mg/kg 2,2,2-tribromoethanol (Sigma-Aldrich, T48402) and 10 mg/kg xylazine (Sigma-Aldrich, X1126). Under anesthesia, an appropriate incision was made in the right posterior part of the mouse to expose the spleen. The mice were placed in the right decubitus position, spleen was pulled out and exposed on the glass plate. The naked abdominal tissues were covered with gauze soaked in saline to prevent the dehydration. During the experiment, mice were placed on a special plate under a constant temperature control at 37 °C and continuously supplemented with the normal saline to prevent the tissue dehydration. For intravital imaging of iNKT and $CD4^+$ T cells, 5 μg of fluorescein-conjugated anti-mouse-CD4 and anti-mouse-CD169 antibodies, respectively were injected into the tail vein. Thereafter, motion trajectories and contact volumes of iNKT and $CD4^+$ T cells were recorded and analyzed using confocal laser scanning microcopy (Zeiss, LSM800, Germany). The Z-stack and video data was analyzed and displayed through Imaris 9.0.1 and Zen 3.3 software.

### Flow cytometry

Flow cytometry analysis of splenic cells and non-parenchymal cells of the liver were performed based on our previously reported protocol[56]. The mice were euthanized and spleen cells were mechanically dissociated with a 70 μm strainer. A single-cell suspension was first incubated with anti-CD16 and anti-CD32 antibodies (BioLegend, San Diego, CA) to block the Fc receptors. To analyze the absolute number of each cell populations, 100 μl of Precision Count Beads were added ($1 \times 10^6$/ml beads, BioLegend, San Diego, CA) into the samples. The single-cell suspension was then washed and resuspended in cold phosphate-buffered saline (PBS), followed by incubation with fluorescein-labeled surface marker antibodies for 30 min at 4 °C in dark. For intracellular cytokine staining, the various samples were pre-treated with PMA/Ionomycin for 4 h (Brefeldin A was added after 2 h), after which the cells were fixed and permeabilized using the BD Fixation/Permeabilization kit (BD, USA) according to the manufacturer's instructions. Sample analysis was performed using a Cytoflex S flow cytometer (Beckman Coulter, USA) and the data were analyzed using FlowJo V10 software (Stanford University, USA) and Cyto Expert V2.4 (Beckman Coulter). Details of the antibodies used in the study are provided in Table S1.

The gating strategy of the cell population relevant to this study is demonstrated in Fig. S8.

### Splenic cell tracing experiment

One hundred microliters of EZ-Link Sulfo-NHS-LC-Biotin (Thermo Fisher, Cat. # 21335, 1 mg/ml) were injected in situ into the mouse spleens. This biotinylates only the surface proteins of whole cells as the negatively charged reagent does not permeate cell membranes. The biotin on the surfaces of the spleen-derived cells was able to bind to the fluorescein-conjugated streptavidin but not to liver-derived cells. After 3 days, non-parenchymal liver cells were prepared using the above method and incubated with antibodies against surface markers and fluorescein-conjugated streptavidin. The percentages of streptavidin-positive cells in the populations of interest were then determined by flow cytometry.

### Mouse $CD4^+$ T cells isolation and RNA-seq

$CD4^+$ T cells were isolated from the mouse spleens (each group consisted of 3 mice) using Mojosort™ CD4 T Cell isolation kit according to the manufacturer's instructions (BioLegend, San Diego, CA). We first added appropriate quantity of TRIzol lysis buffer (Invitrogen, CA, USA) into the cell sample tube (1 mL TRIzol for $1 \times 10^6$ cells) and total RNA was extracted according to the manufacturer's instructions. The transcriptome sequencing and analysis were performed by BGI Genomics (Shenzhen, China). Essentially, differential expression analysis was carried out using the DESeq2 (v1.4.5) with Q value ≤ 0.05 (or FDR ≤ 0.001).

### Gene Annotation

To analyze the changes in phenotype, GO and Kyoto Encyclopedia of Genes and Genomes (KEGG) enrichment analyses of various annotated differentially expressed genes (DEGs) was performed by Phyper based on Hypergeometric test. The significant levels of the terms and pathways were corrected by $P$ value with a rigorous threshold ($P \leq 0.05$). GSEA was carried out using GSEA software.

### Statistics and reproducibility

GraphPad Prism software (Version 9.0, USA) was used for all the statistical analyses. For the comparisons between the two sets of samples, an unpaired t-test with Welch's correction or an unpaired two-tailed Student's t-test was performed. One-way analysis of variance (ANOVA) with a multiple-comparison test was conducted for comparisons among the multiple groups of samples. A threshold of $P < 0.05$ was considered as statistically significant.

For the RNA-seq analysis involved in this study, $n = 3$ mice were used for each group. All samples were independent and groups balanced with controls. The sequencing data was filtered with SOAPnuke by (1) Removing reads whose low-quality base ratio (base quality less than or equal to 15) is more than 20%; (2) Removing reads containing sequencing adapter; (3) Removing reads whose unknown base ('N' base) ratio is more than 5%, afterwards clean reads were obtained and stored in FASTQ format. Expression level of gene was calculated by RSEM (v1.3.1). The heatmap was drawn by pheatmap (v1.0.12) according to the gene expression difference in different samples. Essentially, differential expression analysis was performed using the DESeq2 (v1.4.5) with Q value ≤ 0.05 (or FDR ≤ 0.001).

### Reporting summary

Further information on research design is available in the Nature Portfolio Reporting Summary linked to this article.

## Data availability

All RNA-seq data generated in this work have been deposited into the sequence read archive (SRA) database (PRJNA1022450; PRJNA1180960). Supplementary Video S1 and Video S2 have been stored in the Figshare repository (https://doi.org/10.6084/m9.figshare.28357778). Table S1 has been stored in the Figshare repository (https://doi.org/10.6084/m9.figshare.28365959). All other data used or analyzed during the current study are available from the corresponding author on reasonable request.

Received: 9 April 2024; Accepted: 21 February 2025;
Published online: 03 March 2025

## References

1. Plaz Torres, M. C. et al. Surveillance for hepatocellular carcinoma in patients with non-alcoholic fatty liver disease: universal or selective. *Cancers* **12**, 1422 (2020).
2. Jemal, A. et al. Annual report to the nation on the status of cancer, 1975–2014, featuring survival. *J. Natl Cancer Inst.* **109**, djx030 (2017).
3. Lambert, A. W., Pattabiraman, D. R. & Weinberg, R. A. Emerging biological principles of metastasis. *Cell* **168**, 670–691 (2017).
4. Yang, J. D. et al. A global view of hepatocellular carcinoma: trends, risk, prevention and management. *Nat. Rev. Gastroenterol. Hepatol.* **16**, 589–604 (2019).
5. Forner, A., Reig, M. & Bruix, J. Hepatocellular carcinoma. *Lancet* **391**, 1301–1314 (2018).
6. Pinna, A. D. et al. Liver transplantation and hepatic resection can achieve cure for hepatocellular carcinoma. *Ann. Surg.* **268**, 868–875 (2018).
7. Steeg, P. S. Tumor metastasis: mechanistic insights and clinical challenges. *Nat. Med* **12**, 895–904 (2006).
8. Bronte, V. & Pittet, M. J. The spleen in local and systemic regulation of immunity. *Immunity* **39**, 806–818 (2013).
9. Lewis, S. M., Williams, A. & Eisenbarth, S. C. Structure and function of the immune system in the spleen. *Sci. Immunol.* **4**, eaau6085 (2019).
10. Steiniger, B. & Barth, P. Microanatomy and function of the spleen. *Adv. Anat. Embryol. Cell Biol.* **151**, 1–101 (2000).
11. Allsop, P. et al. Intrasplenic blood cell kinetics in man before and after brief maximal exercise. *Clin. Sci.* **83**, 47–54 (1992).
12. Peters, A. M. Why the spleen is a very rare site for metastases from epithelial cancers. *Med. Hypotheses* **78**, 26–28 (2012).
13. Peters, A. M., Saverymuttu, S. H., Keshavarzian, A., Bell, R. N. & Lavender, J. P. Splenic pooling of granulocytes. *Clin. Sci.* **68**, 283–289 (1985).
14. Brar, S. S. et al. A systematic review of spleen and pancreas preservation in extended lymphadenectomy for gastric cancer. *Gastric Cancer* **15**, S89–S99 (2012).
15. Marasco, G. et al. Role of liver and spleen stiffness in predicting the recurrence of hepatocellular carcinoma after resection. *J. Hepatol.* **70**, 440–448 (2019).
16. Wei, W. et al. Spleen in hepatocellular carcinoma: More complexity and importance than we knew. *J. Hepatol.* **70**, 805–806 (2019).
17. Lee, Y. J. et al. Tissue-specific distribution of iNKT cells impacts their cytokine response. *Immunity* **43**, 566–578 (2015).
18. Dhodapkar, M. V. et al. A reversible defect in natural killer T cell function characterizes the progression of premalignant to malignant multiple myeloma. *J. Exp. Med.* **197**, 1667–1676 (2003).
19. Liu, D. et al. Medulloblastoma expresses CD1d and can be targeted for immunotherapy with NKT cells. *Clin. Immunol.* **149**, 55–64 (2013).
20. Motohashi, S., Okamoto, Y., Yoshino, I. & Nakayama, T. Anti-tumor immune responses induced by iNKT cell-based immunotherapy for lung cancer and head and neck cancer. *Clin. Immunol.* **140**, 167–176 (2011).
21. Tachibana, T. et al. Increased intratumor Valpha24-positive natural killer T cells: a prognostic factor for primary colorectal carcinomas. *Clin. Cancer Res.* **11**, 7322–7327 (2005).
22. Anson, M. et al. Oncogenic β-catenin triggers an inflammatory response that determines the aggressiveness of hepatocellular carcinoma in mice. *J. Clin. Invest.* **122**, 586–599 (2012).
23. Giannou, A. D. et al. Tissue resident iNKT17 cells facilitate cancer cell extravasation in liver metastasis via interleukin-22. *Immunity* **56**, 125–142.e12 (2023).
24. Smyth, M. J. et al. Differential tumor surveillance by natural killer (NK) and NKT cells. *J. Exp. Med* **191**, 661–668 (2000).

25. Ma, C. et al. Gut microbiome-mediated bile acid metabolism regulates liver cancer via NKT cells. *Science* **360**, eaan5931 (2018).
26. Gao, Y. et al. Adoptive transfer of autologous invariant natural killer T cells as immunotherapy for advanced hepatocellular carcinoma: a phase I clinical trial. *Oncologist* **26**, e1919–e1930 (2021).
27. Guo, J. et al. Efficacy of invariant natural killer T cell infusion plus transarterial embolization vs transarterial embolization alone for hepatocellular carcinoma patients: a phase 2 randomized clinical trial. *J. Hepatocell. Carcinoma* **10**, 1379–1388 (2023).
28. Delfanti, G. et al. TCR-engineered iNKT cells induce robust antitumor response by dual targeting cancer and suppressive myeloid cells. *Sci. Immunol.* **7**, eabn6563 (2022).
29. Valente, M. et al. Cross-talk between iNKT cells and CD8 T cells in the spleen requires the IL-4/CCL17 axis for the generation of short-lived effector cells. *Proc. Natl Acad. Sci. USA* **116**, 25816–25827 (2019).
30. Balança, C. C. et al. PD-1 blockade restores helper activity of tumor-infiltrating, exhausted PD-1hiCD39+ CD4 T cells. *JCI Insight* **6**, e142513 (2021).
31. McLane, L. M., Abdel-Hakeem, M. S. & Wherry, E. J. CD8 T cell exhaustion during chronic viral infection and cancer. *Annu. Rev. Immunol.* **37**, 457–495 (2019).
32. Philip, M. et al. Chromatin states define tumour-specific T cell dysfunction and reprogramming. *Nature* **545**, 452–456 (2017).
33. Kaech, S. M. & Ahmed, R. Memory CD8+ T cell differentiation: initial antigen encounter triggers a developmental program in naïve cells. *Nat. Immunol.* **2**, 415–422 (2001).
34. Williams, M. A. & Bevan, M. J. Shortening the infectious period does not alter expansion of CD8 T cells but diminishes their capacity to differentiate into memory cells. *J. Immunol.* **173**, 6694–6702 (2004).
35. Rudloff, M. W. et al. Hallmarks of CD8(+) T cell dysfunction are established within hours of tumor antigen encounter before cell division. *Nat. Immunol.* **24**, 1527–1539 (2023).
36. Good-Jacobson, K. L. Strength in diversity: Phenotypic, functional, and molecular heterogeneity within the memory B cell repertoire. *Immunol. Rev.* **284**, 67–78 (2018).
37. Descatoire, M. et al. Critical role of WASp in germinal center tolerance through regulation of B cell apoptosis and diversification. *Cell Rep.* **38**, 110474 (2022).
38. Dufort, F. J. et al. Cutting edge: IL-4-mediated protection of primary B lymphocytes from apoptosis via Stat6-dependent regulation of glycolytic metabolism. *J. Immunol.* **179**, 4953–4957 (2007).
39. Wurster, A. L., Rodgers, V. L., White, M. F., Rothstein, T. L. & Grusby, M. J. Interleukin-4-mediated protection of primary B cells from apoptosis through Stat6-dependent up-regulation of Bcl-xL. *J. Biol. Chem.* **277**, 27169–27175 (2002).
40. Rush, J. S. & Hodgkin, P. D. B cells activated via CD40 and IL-4 undergo a division burst but require continued stimulation to maintain division, survival and differentiation. *Eur. J. Immunol.* **31**, 1150–1159 (2001).
41. Possamaï, D., Pagé, G., Panès, R., Gagnon, É. & Lapointe, R. CD40L-stimulated B lymphocytes are polarized toward APC functions after exposure to IL-4 and IL-21. *J. Immunol.* **207**, 77–89 (2021).
42. Harris, D. P., Goodrich, S., Mohrs, K., Mohrs, M. & Lund, F. E. Cutting edge: the development of IL-4-producing B cells (B effector 2 cells) is controlled by IL-4, IL-4 receptor alpha, and Th2 cells. *J. Immunol.* **175**, 7103–7107 (2005).
43. Hasbold, J., Lyons, A. B., Kehry, M. R. & Hodgkin, P. D. Cell division number regulates IgG1 and IgE switching of B cells following stimulation by CD40 ligand and IL-4. *Eur. J. Immunol.* **28**, 1040–1051 (1998).
44. Chakma, C. R. & Good-Jacobson, K. L. Requirements of IL-4 during the generation of B cell memory. *J. Immunol.* **210**, 1853–1860 (2023).
45. Fridman, W. H. The tumor microenvironment: Prognostic and theranostic impact. Recent advances and trends. *Semin. Immunol.* **48**, 101416 (2020).
46. Sautès-Fridman, C. et al. Tertiary Lymphoid Structures and B cells: clinical impact and therapeutic modulation in cancer. *Semin. Immunol.* **48**, 101406 (2020).
47. Downs-Canner, S. M., Meier, J., Vincent, B. G. & Serody, J. S. B cell function in the tumor microenvironment. *Annu. Rev. Immunol.* **40**, 169–193 (2022).
48. Sarvaria, A., Madrigal, J. A. & Saudemont, A. B cell regulation in cancer and anti-tumor immunity. *Cell Mol. Immunol.* **14**, 662–674 (2017).
49. Mao, Y. et al. Circulating exosomes from esophageal squamous cell carcinoma mediate the generation of B10 and PD-1(high) Breg cells. *Cancer Sci.* **110**, 2700–2710 (2019).
50. Engelhard, V. et al. B cells and cancer. *Cancer Cell* **39**, 1293–1296 (2021).
51. Lehmann, J., et al. Tertiary lymphoid structures in pancreatic cancer are structurally homologous, share gene expression patterns and B-cell clones with secondary lymphoid organs but show increased T-cell activation. *Cancer Immunol. Res.* https://doi.org/10.1158/2326-6066.CIR-24-0299 (2024). Epub ahead of print.
52. Lella, R. K. & Malarkannan, S. IQGAP1 promotes early B cell development, is essential for the development of marginal zone (MZ) B cells, and is critical for both T-dependent and T-independent antibody responses. *Cell Mol. Life Sci.* **81**, 462 (2024).
53. Smith, T. J. et al. Engineered IgM and IgG cleaving enzymes for mitigating antibody neutralization and complement activation in AAV gene transfer. *Mol. Ther.* **32**, 2080–2093 (2024).
54. Lacoste, B., Raymond, V. A., Cassim, S., Lapierre, P. & Bilodeau, M. Highly tumorigenic hepatocellular carcinoma cell line with cancer stem cell-like properties. *PLoS ONE* **12**, e0171215 (2017).
55. Ni, R. et al. A mouse model of irradiation and spleen-thymus lymphocyte infusion induced aplastic anemia. *Hematology* **27**, 932–945 (2022).
56. Han, M. et al. Invariant natural killer T cells drive hepatic homeostasis in nonalcoholic fatty liver disease via sustained IL-10 expression in CD170(+) Kupffer cells. *Eur. J. Immunol.* **53**, e2350474 (2023).


## Acknowledgements

We thank the NIH Tetramer Core Facility for providing the CD1d-PBS57-Tetramer reagent. We thank Professor Yuanli Chen (Hefei University of Technology, Hefei, China) for providing the IFN-$\gamma^{-/-}$ mice. Parts of the graphical abstract were drawn by using pictures from Servier Medical Art. Servier Medical Art by Servier is licensed under a Creative Commons Attribution 3.0 Unported License (https://creativecommons.org/licenses/by/3.0/). We thank MJEditor (www.mjeditor.com) for providing English editing services during the preparation of this manuscript. This work was funded by the Suzhou "KeJiaoQiangWei" Youth Project (QNXM2024034), the Young Talent Development Project (GSKY20240511), the Gusu Health Talent Project (2024-180), the Scientific Research Project of Jiangsu Commission of Health (M2022127), Suzhou Science and Technology Demonstration Project (SS202005), National Natural Science Foundation of China (82271696, 82101902) and Natural Science Foundation of Jiangsu Province (BK20201079).

## Author contributions

Conceptualization: M.H. Investigation: J.G., M.H., M.X., M.Y., X.X., F.W., and R.Z. Data curation and formal analysis: M.H. and J.G. Writing—original draft: M.H. Writing—review, editing, and revision: M.H. and R.Z. All authors read and approved the final manuscript.

## Competing interests

The authors declare no competing interests.

## Ethics approval and consent to participate

The research project has been reviewed and approved by the Institutional Animal Care and Use Committee of Nanjing Medical University Affiliated

Suzhou Hospital, in line with the Basel Declaration and the welfare and ethical principles of laboratory animals (Project number K-2024-047).

## Additional information

**Supplementary information** The online version contains supplementary material available at https://doi.org/10.1038/s42003-025-07798-2.

**Correspondence** and requests for materials should be addressed to Rui Zhu or Mutian Han.

**Peer review information** *Communications Biology* thanks the anonymous reviewers for their contribution to the peer review of this work. Primary Handling Editor: Christina Karlsson Rosenthal.